REVIEW

Work function optimization for enhancement of sensitivity of dual-material (DM), double-gate (DG), junctionless MOSFET-based biosensor

Monika Kumari[1] · Niraj Kumar Singh[1] · Manodipan Sahoo[1] · Hafizur Rahaman[2]

Abstract

In this work, the impact of gate material work function on the sensitivity of dual-material, double-gate, junctionless MOS-FET ($DMDG - JL - MOSFET$)-based biosensor has been studied. To enhance the sensitivity of the biosensor, optimization of gate work functions has been done through Sentaurus TCAD simulator. With the immobilization of biomolecules in the cavity at different value of work function of gate metal 1 ($M1$) and gate metal 2 ($M2$), i.e., $WF1$ and $WF2$, enhancement in sensing metrics (change in threshold voltage S_{Vth} and I_{ON}/I_{OFF} ratio) is observed. The enhancement in sensitivity is profound in source-side gate (M1) work function (WF1) optimization as compared to drain-side gate (M2) work function (WF2) optimization. Sensitivity of 90 mV is observed in source-side gate work function optimization which is ∼ 89% more than the sensitivity of 23 mV which is achieved in drain-side gate work function optimization for a fixed concentration and dielectric constant of biomolecules. It has also been noted that the proposed structure exhibits ∼ 90% higher sensitivity than the single-material, dual-gate, junctionless MOSFET ($SMDG - JL - MOSFET$) biosensor. Results showcase that the optimization of gate metal work functions enhances the sensitivity of the biosensor.

Keywords Work function · DMDG-JL-MOSFET · Biosensor · Sentaurus TCAD · Sensitivity · SMDG-JL-MOSFET

1 Introduction

Biosensors have vast application in the field of biomedical, food processing, point-of-care treatment and in many more areas. FET-based biosensors have been extensively used in these areas for the label-free detection of biomolecules, because of their small size, low weight, low-cost mass production and the possibility of on-chip integration of both sensor and measurement systems [1–4]. With the evolution of CMOS technology, scaling of conventional MOSFET has given rise to challenges in fabrication of short-channel MOSFET-based biosensors [5]. Junctionless (JL) MOS-FET has been proposed as one of the potential alternative to overcome this problem [6–8]. Junctionless devices have uniform doping from source to channel to drain and does not have any junction. It makes $JL - MOSFET$ easy to fabricate, reduces SCEs and improves I_{ON}/I_{OFF} ratio of the device [9, 10]. Moreover, manufacturing of $JL - MOSFET$ is simpler as it does not require high thermal budget since the doping is homogeneous. These qualities of $JL - MOSFET$ are advantageous for the fabrication of miniaturized sensor devices and their heterogeneous integration with other components for noninvasive clinical diagnostics, and disposable applications [11]. Till now, different types of FET-based biosensors have been explored. Narang et al. [12] has reported dielectrically modulated FET ($DM - FET$)-based biosensor with an analytical model. An experimental demonstration of nanogap-embedded biosensor has already been performed [2]. Choi et al. [13] reported analytical modeling

✉ Monika Kumari
  kumarimonika975@gmail.com

  Niraj Kumar Singh
  nirajkrssingh4@gmail.com

  Manodipan Sahoo
  manodipan@iitism.ac.in

  Hafizur Rahaman
  rahaman.h@gmail.com

[1] Department of Electronics Engineering, Indian Institute of Technology (Indian School of Mines), Dhanbad, Jharkhand 826004, India

[2] Department of Information Technology, IIEST, Shibpur, Howrah 711103, India

of biosensor based on $DM - FET$. Buitrago et al. [11] have proposed junctionless transistors with SOI structure for low-power sensors with high sensitivity. Apart from fabrication challenges of biosensors at nanoscale dimensions, to get better drive current and ultrasensitivity, dual-material double-gate ($DMDG$) MOSFET has been suggested. Dual-material gate (DMG) MOSFET was first reported by Wei Long and K. K. Chin [14]. DMG structure has two different gate materials for better gate control and enhancement of sensitivity. Such a configuration provides a reduction in off current due to a step in the surface potential profile when compared with a single-material gate (SMG) MOSFET structure which is helpful in increasing the sensitivity of the biosensor. Ahangari et al. [4] has reported a dual-material gate, junctionless, nanowire MOSFET-based sensor for low power and ultrahigh sensitivity. The DMG structure ensures higher control of gate over the conductance of the channel which increases the gate transport efficiency and enhances the sensitivity of the device. The channel region under the gate metal 1 on the source side is screened from drain potential variations due to the step function profile of the surface potential. Narang et al. [12] has reported single-material double-gate $JL - MOSFET$-based biosensor. Ajay et al. [15] has reported gate underlap $JL - MOSFET$-based biosensor with single-sided cavity. Singh et al. [16] has reported split gate-$JL - MOSFET$-based biosensor. To incorporate the advantages of $JL - MOSFET$, dual-material gate (DMG) structure and gate stack engineering and to enhance the sensitivity of $JL - MOSFET$-based biosensor, $DMDG - JL - MOSEFT$-based label-free biosensor [17–19] has been proposed as depicted in Fig.1. Lakshmi et al. [20] has analyzed the impact of gate work function variation on the performance of $JL - MOSFET$ for analog applications. Praveen et al. [21] has studied the effect of gate work function variation on sensitivity of tunnel FET biosensors. Here, optimization of gate material work function has been done to find out the suitable range of gate material work function for

which the sensitivity of the label-free biosensor is enhanced. Principal contributions of this work are

– Different work functions of gate metal 1 and metal 2 which are compatible with the CMOS technology have been chosen and optimized to achieve maximum sensitivity of the biosensor. To simulate the characteristics of the device, Sentaurus TCAD simulator has been used [22].
– Effect of gate work function on the sensitivity of the device has been studied by varying the dielectric constant of biomolecules.
– We have studied the effect of work function variation of gate metal 1 ($WF1$) and keeping the work function of gate metal 2 ($WF2$) fixed and the variation of work function of gate metal 2 and keeping the work function of gate metal 1 fixed, on surface potential, threshold voltage (V_{th}) and I_{ON}/I_{OFF} ratio of the proposed device.

The rest of the paper is organized as follows. In section 2, the device structure is explained in detail. Section 3 describes the methodology adopted for simulation. Section 4 discusses the results in detail. Finally, the conclusions are drawn in Sect. 5.

2 Device structure

The device architecture of a dielectrically modulated, $DMDG - JL - MOSFET$-based biosensor is presented in Fig. 1. For dual-material gate, gate region is equally divided into two parts, Gate 1 and Gate 2. In addition, materials with higher work function are chosen as the gate material 1, which is close to the source, and materials with lower work function are chosen as gate material 2, which is close to the drain. The set of work functions of gate 1 and gate 2 used for the simulation are mentioned in Tables 1 and 2. Here, L_1 is the length of gate 1 and L_2 is the length of gate 2, L_3 and
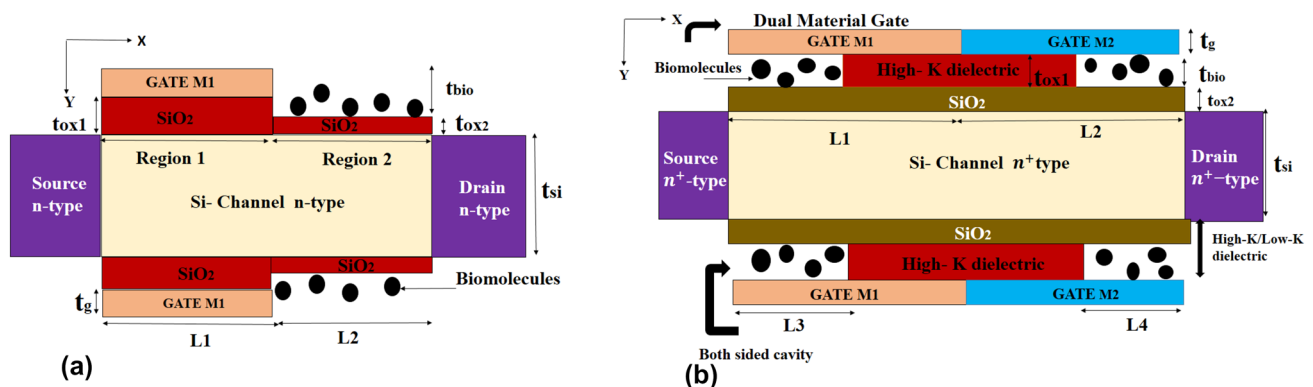

Fig. 1 **a** Device structure of JL-MOSFET-based biosensor with single-side cavity [15]; **b** device structure of DMDG-JL-MOSFET-based biosensor (our work)

Table 1 Work function of gate metal 2(*M*2) for a fixed value of work function for gate metal 1 (*M*1)

WF1 (eV)	Range of WF2(eV)
5.1	3.9 − 5.1
5.2	3.9 − 5.2
5.3	3.9 − 5.3
5.4	3.9 − 5.4

Table 2 Work function of gate metal 1 (*M*1) for a fixed value of work function for gate metal 2 (*M*2)

WF2 (eV)	Range of WF1(eV)
4.2	4.2 − 5.5
4.3	4.3 − 5.5
4.4	4.4 − 5.5
4.5	4.5 − 5.5

L_4 are the lengths of the nanogap cavity in which biomolecules get immobilized. High-κ/low-κ dielectric material as gate oxide stack is used to improve the sensing performance of the device. Here, HfO_2 is used as high-κ gate oxide and SiO_2 is used as low-κ gate oxide. T_{bio}, T_{Si}, T_{ox1} and T_{ox2} are the thicknesses of the nanogap cavity, silicon channel, high-κ dielectric material and low κ dielectric material, respectively. In this work, the length of cavity (L_{cav}) is considered as 25 nm. In [23], size of protein biomolecules reported is in deca-nanometer range and the size of biotin and streptavidin is nearly 5 nm [24]. Moreover, the experimental demonstration of trapping of streptavidin within 10 nm cavity has been shown by Kim et al. [25]. Hence, thickness of nanogap is taken to be 9 nm in this work. A SiO_2 layer of thickness 1 nm is used as low κ dielectric material in this work. SiO_2 layer is also considered in the nanogap cavity region because it works as an adhesive layer for the biomolecules to get immobilized in the nanocavity whenever silicon substrate is exposed to the air [26]. Various device parameters used in this work are presented in Table 3.

3 Simulation methodology

In this work, Sentaurus TCAD simulator has been used [22] for the simulation purpose. Models used in TCAD simulations are drift–diffusion model (DD) for carrier transport, FERMI DIRAC model for carrier characteristics, FLDMOB model for field-dependent mobility, Shockley–Read–Hall (SRH) model along with AUGER combination model for carrier generation and recombination in the highly doped channel of the device, constant mobility model, Lombardi constant voltage and temperature (CVT) model and Boltzmann transport model. Quantum effects have been ignored in the simulation [27]. To gain insight into the behavior of the proposed device, different values of gate material work functions are analyzed with biomolecules immobilized in the cavity. The presence of the neutral biomolecules in the nanogap cavity is simulated by introducing material having dielectric constants ($\kappa > 1$) corresponding to the biomolecules (e.g., dielectric constants are streptavidin=2.1 [28], protein = 2.50, biotin = 2.63 [29] and APTES = 3.57 [30]). For a given fixed value of $WF1$, $WF2$ value is varied and for a given fixed value of $WF2$, $WF1$ is varied and characteristics of the device are simulated.

4 Results and discussion

The effect of variations of gate metal work function on surface potential and on sensitivity metrics is plotted and discussed in this section. The simulated data are calibrated with the data in [12], and it is closely matched as it can be observed in Fig. 2. We have selected the work functions of gate metal 1 and metal 2 which are compatible with the CMOS technology. For gate work functions optimization, first $WF2$ is varied keeping $WF1$ fixed and then $WF1$ is varied keeping $WF2$ fixed. The bound is when $WF2 = WF1$ (i.e., when the dual-material gate structure characteristics correspond to single-material gate characteristics). Biomolecules with dielectric constants ($\kappa= 3,5,7,9,12$) have been chosen to vividly observe the effect of biomolecules on the characteristics of the proposed $DMDG − JL − MOSFET$ -based biosensor.

Figure 3a, b depicts the change in surface potential with the variation in $WF2$ when $WF1$ is kept fixed and when $WF1$ is varied and $WF2$ is kept fixed, respectively, at biomolecule dielectric constant of $\kappa=12$. It can be observed that the $DM − DG$ structure exhibits a step function in the surface potential at the transition from gate metal-1 to metal-2. This abrupt change is caused by the difference of work function of gate metals [31, 32]. Due to this unique feature, the area under the gate metal 1 of the $DM − DG$ structure is screened from the drain potential variations; it reduces the drain conductance and DIBL. A large δWF between the work functions of two gate materials leads to an improvement in the carrier transport efficiency. It can be observed from Fig. 3a that as $\delta WF=(WF1 − WF2)$ increases the step profile of potential increases, but the source-side barrier is not altering with the change of $WF2$, whereas, in Fig.3b, source-side barrier changes significantly with $WF1$ variations. With the increase in $WF1$, δWF increases and there is an enhancement in the threshold voltage of the device due to increasing value of $WF1$ [31, 33], which improves sensitivity of the biosensor change. When $WF2$ becomes equal to $WF1$ (i.e., $\delta WF=0$), the surface potential shows the profile of $SM − DG$ structure.

Threshold voltage is an important sensing metric of FET-based biosensors to detect the sensitivity when biomolecules are immobilized in the cavity. Figure4a, b depicts

the variation in threshold voltage with a change in *WF*2 for a fixed value of *WF*1 and with a change in *WF*1 for a fixed value of *WF*2, respectively, with dielectric constant $\kappa = 12$. When biomolecules with dielectric constant ($\kappa > 1$) are accumulated in the cavity, the gate capacitance increases. This variation of gate capacitance leads to higher effective coupling between gate and channel, which results in a decrease in central channel potential [34]. This depicts the requirement of higher gate voltage to deplete the channel completely, thereby causing an increase in threshold voltage compared to air-filled cavity. In Fig. 4a, when the work function (*WF*2) of drain-side gate (M2) is varied, keeping *WF*1 fixed, the step profile of the potential changes, but the change in threshold voltage is minimal; it is because there are insignificant variations in source channel barrier height. In Fig.4b, when the work function (*WF*1) of source-side gate M1 is varied, keeping *WF*2 fixed the step profile of the potential varies and the variation in threshold voltage is significant; it is because of the variations in source-side barrier; thus, the threshold voltage requirement of carriers to cross the source-side barrier shows notable change. Moreover, When the difference between *WF*1 and *WF*2 is higher, the observed threshold voltage is also higher [14, 31, 32]. It can be observed from 4a that the threshold voltage is 0.718*V* when δWF is 1.2 *eV*, and when the value of δWF decreases, threshold voltage decreases only with a minimal value of 0.012 *V*, whereas, in Fig. 4b the threshold voltages are 0.941*V* and 0.2*V* at $\delta WF = 1eV$ and at $\delta WF = 0.2eV$, respectively. So the change in threshold voltage is 0.74*V*.

Here, Fig. 5 shows the sensitivity of the proposed device with the variation in *WF*2 for a fixed value of *WF*1 (Fig. 5a) and *WF*1 for a fixed value of *WF*2 (Fig. 5b), for biomolecules with $\kappa = 7$ and 12. Sensitivity of a device for neutral biomolecules is expressed as

$S_{Vth} = V_{th}(\kappa > 1) - V_{th}(\kappa = 1)$. For ($\kappa = 12$), in Fig. 5a maximum sensitivity of 23 mV is observed for *WF*2 = 4.1 eV and for ($\kappa = 7$), maximum sensitivity of 16 mV is observed at a *WF*2 of 4.1 eV and in Fig. 5b the maximum sensitivity of 88 mV is observed at *WF*1= 5.5 eV and minimum sensitivity of 21 mV is observed at *WF*1= 4.2 eV, for ($\kappa = 7$), maximum sensitivity of 62 mV is observed at a *WF*2 of 5.5 eV and minimum sensitivity of 9 mV is observed at *WF*1= 4.2 eV.

I_{ON}/I_{OFF} ratio of the device is shown in Fig. 6, which is considered as another sensing metric for a FET-based biosensor. As δWF increases, the I_{ON}/I_{OFF} ratio of the device increases [31, 32]. The reason behind these phenomena is as δWF increases, the effect of control gate (M1) on the channel increases which in turn results in an increase in threshold voltage and subsequently off current decreases and thus I_{ON}/I_{OFF} ratio increases. With an increase in dielectric constant of the biomolecules in the cavity region, I_{ON}/I_{OFF} ratio increases which is clearly depicted in Fig. 6.

Table 3 Physical parameters of DMDG-JL-MOSFET

Device parameter	Value
Channel length (L_{ch})	100 nm
Length of gate1 (L_1) and gate 2 (L_2)	50 nm
Length of cavity (L_3 and L_4)	25 nm
High-κ gate oxide thickness (T_{ox1})	9 nm
Channel thickness (T_{Si})	10 nm
Nanogap thickness (T_{bio})	9 nm
Low-κ gate oxide thickness (T_{ox2})	1 nm
Source and drain doping concentration (N_{sd})	$10^{19}\ cm^{-3}$
Channel doping concentration (N_d)	$10^{19}\ cm^{-3}$

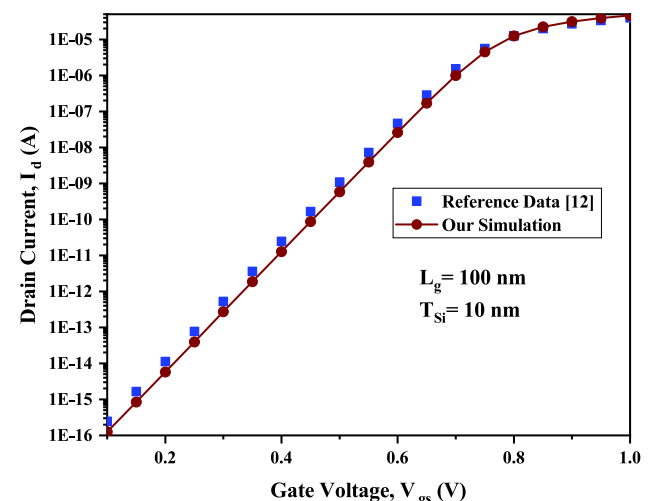**Fig. 2** Calibration of our simulated $I_D - V_G$ data with $I_D - V_G$ data of [12].($V_{gs} = 1\ V$ and $V_{ds} = 0.05V$.)

Figure 6a shows the I_{ON}/I_{OFF} when the work function of drain-side gate metal (M2) is varied with *WF*1 constant. Since there is not considerable change in the threshold voltage, the change in I_{ON}/I_{OFF} is also not significant in this case. Figure 6b shows the I_{ON}/I_{OFF} when the work function of source-side gate metal (M1) is varied with fixed *WF*2.

Figure 7 shows the step function profile for *DMDG − JL − MOSFET*-based biosensor for different biomolecules with different dielectric constants ($\kappa = 5, 7, 10, 12$). *WF*1 and *WF*2 are chosen as 5.3 and 3.9 eV, respectively, for this plot. Deformation in potential profile appears when the cavity is filled with biomolecules. Deformation in potential profile is more at the source side; this is due to the fact that, for certain type of biomolecules, the channel under higher work function gate metal gets strongly depleted due to stronger electrostatic coupling between gate and channel region [12]. Moreover, as the dielectric constant increases, the height of step profile increases, which means control of gate material 1 on the
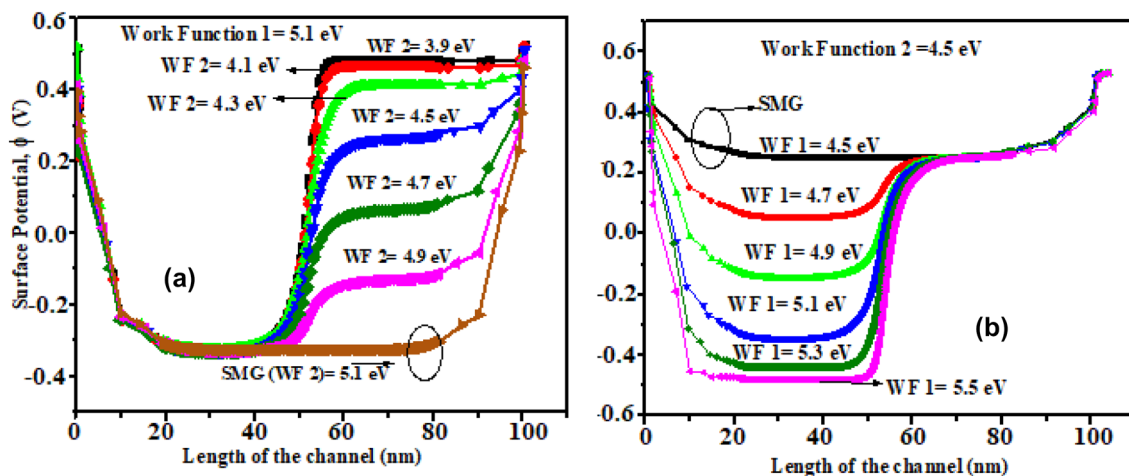
Fig. 3 Change in surface potential with **a** WF2 variation for a fixed WF1 and **b** WF1 variation for a fixed WF2. ($V_{gs} = 1$ V , $V_{ds} = 0.05V$ and $\kappa = 12$)
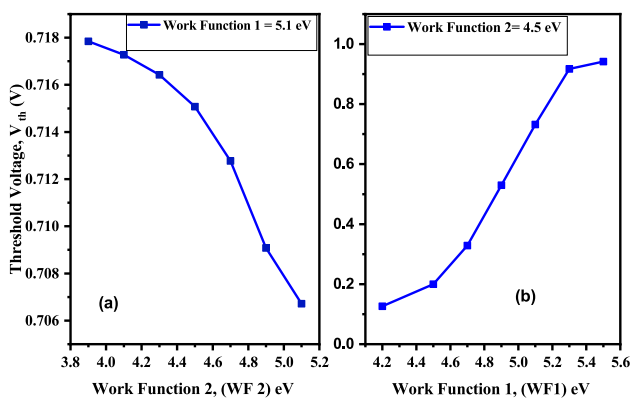

Fig. 4 Change in threshold voltage with **a** WF2 variation for a fixed WF1 and **b** WF1 variation for a fixed WF2 with biomolecules having dielectric constant ($\kappa = 12$)
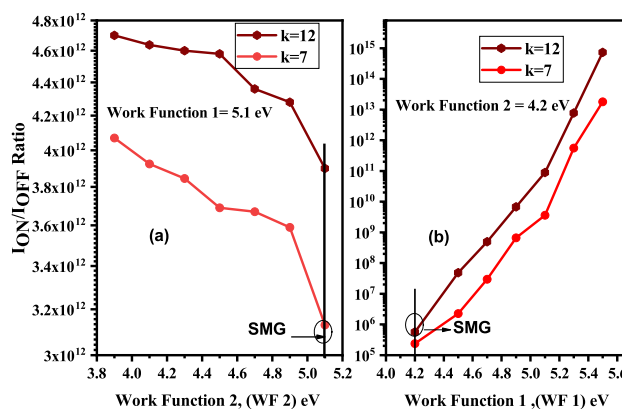

Fig. 6 I_{ON}/I_{OFF} ratio with **a** WF2 variation for a fixed WF1 and **b** WF1 variation for a fixed WF2 with biomolecules having ($\kappa = 7$, 12)
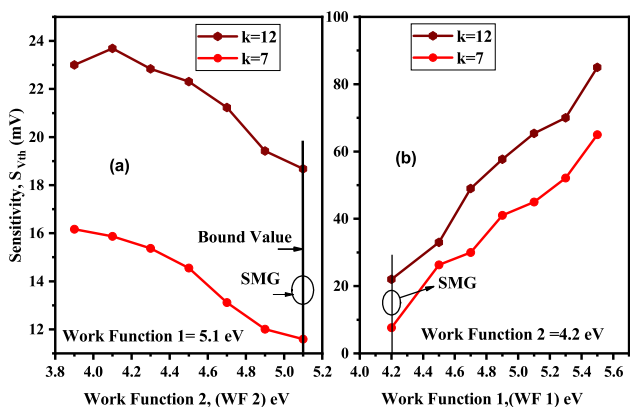

Fig. 5 Change in sensitivity with **a** WF2 variation for a fixed WF1 and **b** WF2 variation for a fixed WF1 with biomolecules having ($\kappa = 7$, 12)

channel strengthens [31, 35] which results in improvement in sensitivity of the device.

Figure 8a shows the threshold voltage variation of the device for $\kappa = 12$. WF1 is fixed at 5.3 eV and WF2 is varied. Figure 8b shows the threshold voltage variation of the device for $\kappa = 12$. WF2 is fixed at 4.5 eV and WF1 is varied. For drain-side work function variations, change in threshold voltage is less, and for source-side work function variation, change is threshold voltage is considerable and the reasoning is mentioned earlier. For WF2 = 3.9 eV and fixed value of WF1= 5.3 eV, maximum value of the threshold voltage observed is 0.909V. For WF1 = 5.5 eV and fixed value of WF2= 4.5 eV, maximum value of the threshold voltage observed is 0.941V.

It can be observed from Fig. 9a the sensitivity variation of the device for biomolecules having dielectric constants, $\kappa = 7$ and 12, with the change in WF2 for a fixed value of
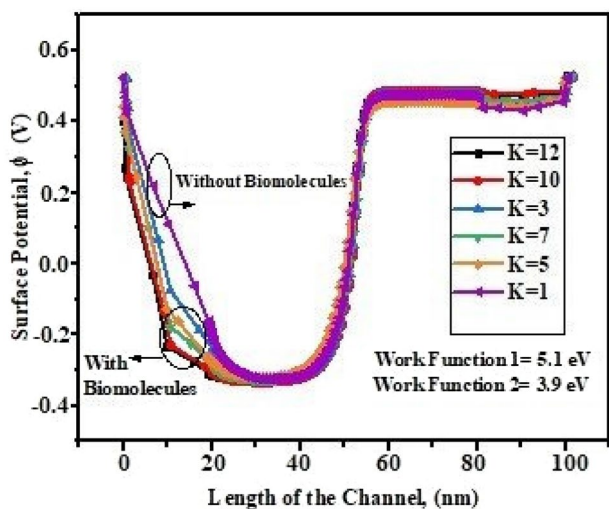
Fig. 7 Change in surface potential for different dielectric constants of biomolecules with $\delta WF = 1.4\ eV$. ($V_{gs} = 1\ V$ and $V_{ds} = 0.05V$)
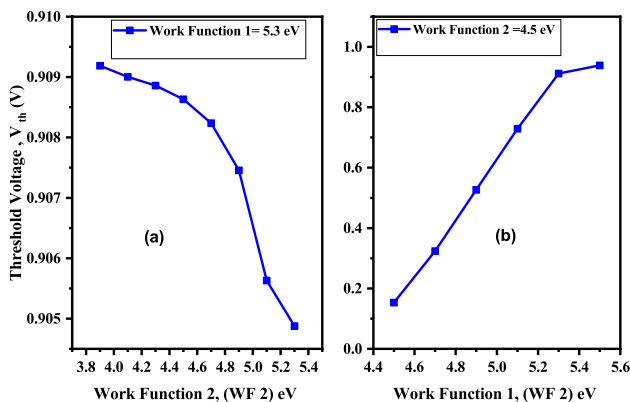

Fig. 8 Change in threshold voltage with **a** $WF2$ variation for a fixed $WF1$ and **b** $WF1$ variation for a fixed $WF2$ with biomolecules having ($\kappa = 12$)
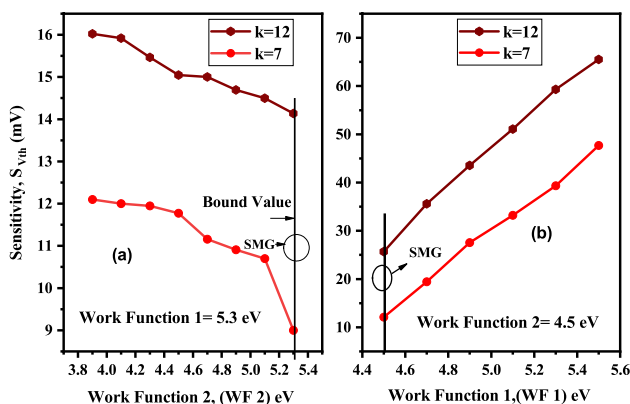

Fig. 9 Change in threshold voltage with **a** $WF2$ variation for a fixed $WF1$ and **b** $WF1$ variation for a fixed $WF2$ with dielectric constant of biomolecules ($\kappa = 7, 12$)
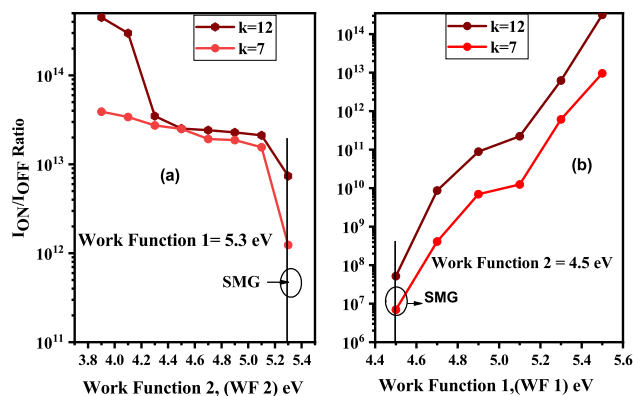

Fig. 10 I_{ON}/I_{OFF} ratio with **a** $WF2$ variation for a fixed $WF1$ and **b** $WF1$ variation for a fixed $WF2$ with biomolecules having ($\kappa = 7, 12$)

Table 4 Work function of gate M1 and M2

$WF1$ (eV)	Optimum range of $WF2$ (eV)	Maximum sensitivity, $S_V th$ (mV)
5.2	$4.2 - 4.9$	21
5.4	$4.4 - 5$	15
5.5	$4.5 - 5.1$	13

Table 5 Work function of gate M1 and M2

$WF2$ (eV)	Optimum range of $WF1$ (eV)	Maximum sensitivity, $S_V th$ (mV)
4.1	$4.1 - 5.4$	92
4.3	$4.3 - 5.5$	80
4.4	$4.4 - 5.1$	78

$WF1 = 5.3$ eV, and Fig. 9b shows the variation in sensitivity when $WF2$ is kept fixed at 4.5 eV and $WF1$ is varied. It can be observed that sensitivity is more for higher dielectric constant of biomolecules and it increases with the an increase in δWF. Here, the calculated sensitivity is 16 mV which is the highest among all for $WF2 = 3.9$ eV for drain-side gate (M2) work functions variations, and 66 mV of sensitivity is achieved at $WF1 = 5.5$ eV for source-side gate (M1) work functions variations.

With an increase in dielectric constant of the biomolecules in the cavity region as well as with the increase in δWF, I_{ON}/I_{OFF} ratio increases which is clearly depicted in Fig. 10. At last, it can be observed from the above discussion that high sensitivity ($S_V th$) and high I_{ON}/I_{OFF} ratio (which are the two important sensing metrics for a biosensor) are achieved, when the work function of source-side gate metal (M1) is varied keeping $WF2$ fixed as compared to drain-side
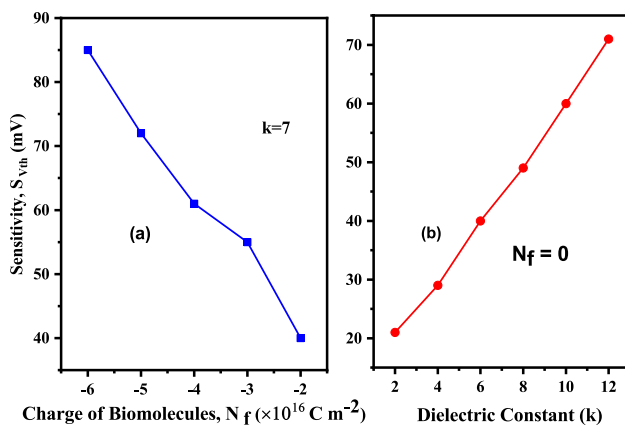
Fig. 11 Change in sensitivity for $WF1$= 5.5 eV and $WF2$= 4.2 eV with the variation in **a** dielectric constant (κ) of neutral biomolecules and **b** charge of charged biomolecules

metal gate (M2) work function variation with $WF1$ fixed. However, choosing a very high δWF can also cause significant reliability issues that are not desirable for nanodevices and especially for biosensors [36]. Thus, for a given value of $WF1$, an optimum range of $WF2$ (Table 4) and for a given value of $WF2$, an optimum range of $WF1$ (Table 5) is found out to achieve enhanced sensitivity of the device.

The proposed DM-DG-JL-MOSFET-based biosensor is a label-free biosensor. It can distinguish between different biomaterials using their dielectric constant (k) and charge density (C m^{-2}). Figure 11a shows the sensitivity plot of the device with the variation in dielectric constant (κ) of neutral biomolecules. Figure 11b shows the sensitivity plot of the proposed structure with the variation in charge of charged biomolecules. It can be observed from both the figures that there is a change in sensitivity with the variation in dielectric constant and charge of biomolecules. The proposed DM-DG-JL-MOSFET-based biosensor can distinguish between biomaterials using the sensitivity parameter, i.e., dielectric constant(κ) and charge of biomolecules [15, 19].

5 Conclusion

In this work, we have investigated the optimization of work function of gate materials of a $DMDG - JL - MOSFET$-based biosensor for enhancement in the sensitivity of the device. It has been found that by varying the work function of source-side gate metal (M1) and keeping the work function of drain-side gate metal (M2) fixed, the sensitivity of the device is enhanced profoundly as compared to the change in work function of drain-side gate metal (M2) and keeping the work function of source-side gate metal (M1) fixed. When $WF1$ is varied, work function difference δWF significantly impacts the characteristics and sensitivity of

the biosensor by modulating the ability of gate to control the channel. It has been observed that $WF1 = 5.5\ eV$ and $WF2 = 4.2\ eV$ show the maximum sensitivity for the device. The proposed structure also shows $\sim 90\%$ improvement in sensitivity compared to single-material, dual-gate ($SM - DG$) structure with same parameters. A range of optimum values of $WF1$ for a fixed value of $WF2$ and a range of optimum values of $WF2$ for a fixed value of $WF1$ has also been found out to achieve optimum sensitivity for the proposed biosensor.

References

1. P. Bergveld, The development and application of FET-based biosensors. Biosensors. **2**(1), 15–33 (1986)
2. H. Im, X.-J. Huang, B. Gu, Y.-K. Choi, A dielectric-modulated field-effect transistor for biosensing. Nat. Nanotechnol. **2**(7), 430–434 (2007)
3. C.H. Kim, C. Jung, H.G. Park, Y.K. Choi, Novel dielectric modulated field-effect transistor for label-free DNA detection. Biochip J. **2**(2), 127–134 (2008)
4. B. Gu, T.J. Park, J.-H. Ahn, X.-J. Huang, S.Y. Lee, Y.-K. Choi, Nanogap field-effect transistor biosensors for electrical detection of avian influenza. Small **5**(21), 2407–2412 (2009)
5. H. Wong.:Beyond the conventional MOSFET, Proceeding of 31th European Solid State Device Research Conference (69)5
6. A. Afzalian, N. Akhavan.: Junctionless multigate field-effect transistor, Appl.Phys.Lett. **94**(5), 053511 (2009)
7. J.P. Colinge, C. Lee.: Reduced electric field in junctionless transistors, Appl.Phys.Lett. **94**(7), 073510 (2010)
8. C.-W. Lee, N.D. Akhavan, High-temperature performance of silicon junctionless MOSFETs. IEEE Trans. Electron Devices **57**(3), 620–625 (2010)
9. C. Li, Y. Zhuang, R. Han, Subthreshold behavior models for nanoscale short-channel junctionless cylindrical surrounding-gate MOSFETs. IEEE Trans. Electron Devices. **60**(11), 3655–3662 (2013)
10. T. Wang, L. Lou, C. Lee, A junctionless gate-all-around silicon nanowire FET of high linearity and its potential applications. IEEE Trans. Electron Devices **34**(4), 478–480 (2013)
11. E. Buitrago, F. Giorgos, M. Badia, M.B.Y.M. Georgiev, A.M. Ionescu, Junctionless silicon nanowire transistors for the tunable operation of a highly sensitive, low power sensor. Sens. Actuat. B: Chem. **183**, 1–10 (2013)
12. S. Ajay, R. Narang, M. Saxena, M. Gupta, Investigation of dielectric modulated (DM) double gate (DG) junctionless MOSFETs for application as a bio-sensors. Superlattices Microstruct. **85**, 557–572 (2015)
13. J.M. Choi, J.W. Han, S.J. Choi, Y.K. Choi, Analytical modeling of a nanogap-embedded FET for application as a biosensor. IEEE Trans. Electron Devices **57**(12), 3477–3484 (2010)
14. W. Long, K.K. Chin.:Dual material gate field effect transistor (dmg fet), International Electron Devices Meeting., IEDM Technical Diges

15. Ajay, R. Narang, Modeling of gate underlap junctionless double gate mosfet as bio-sensor. Mater. Sci. Semicond. Process. **71**, 240–251 (2017)

16. S. Singh, B. Raja, Analytical modeling of split-gate junction-less transistor for a biosensor application. Sens. Bio-Sens. Res. **18**, 31–36 (2018)

17. M. Curreli, R. Zhang, F.N. Ishikawa, H.-K. Chang, R.J. Cote, C. Zhou, M.E. Thompson, Real-time, label-free detection of biological entities using nanowire-based FETs. IEEE Trans. Nanotechnol. **7**(6), 651–667 (2008)

18. A. Syahir, K. Usui, K.-Y. Tomizaki, K. Kajikawa, H. Mihara, Label and label-free detection techniques for protein microarrays. Microarrays **4**, 228–244 (2015)

19. Y. Ohno, K. Maehashi, K. Matsumoto, Label-free biosensors based on aptamer-modified graphene field-effect transistors. J. Am. Chem. Soc. **132**, 18012–18013 (2010)

20. B. Lakshmi, R. Srinivasan, Performance analysis of dual metal gate work function in junctionless transistors. J. Comput. Theor. Nanosci. **10**(6), 1354–1358 (2013)

21. P. Dwivedi, R. Singh, Investigation the impact of the gate work-function and biases on the sensing metrics of tfet based biosensors. Eng. Res. Express

22. TCAD Sentaurus Device User Manual, Synopsys, CA (2013)

23. M.S. Parihar, D. Ghosh, G.A. Armstrong, P. Razavi, A. Kranti, Bipolar e ects in unipolar junctionless transistors. Appl. Phys. Lett. **101**, 093507 (2012)

24. D.Y. Jang et al., Sublithographic vertical gold nano-gap for label-free electrical detection of protein ligand binding. J. Vac. Sci. Technol. B **25**, 443–447 (2007)

25. S. Kim, J.-H. Ahn, T.J. Park, S.Y. Lee, Y.-K. Choi, A biomolecular detection method based on charge pumping in a nanogap embedded eld-e ect-transistor biosensor, Appl. Phys. Lett. **94**(24), 243903 (2009)

26. K.-W. Lee, S.-J. Choi, J.-H. Ahn, D.-I. Moon, T.J. Park, S.Y. Lee, Y.- K Choi, An underlap eld-e ect transistor for electrical detection of influenza. Appl. Phys. Lett. **96**(3), 033703 (2010)

27. M. S. Lundstrom, Essential physics of carrier transport in nanoscale mosfets. IEEE Trans. Electron. Devices **49**, 133–141 (2002)

28. S. Busse, V. Scheumann, B. Menges, S. Mittler, Sensitivity studies for speciic binding reactions using the biotin/streptavidin system by evanescent optical methods. Biosens. Bioelectron. **17**(8), 704–710 (2002)

29. A. Densmore, D.-X. Xu, S. Janz, P. Waldron, T. Mischki, G. Lopinski, A. Delge, J. Lapointe, P. Cheben, B. Lamontagne, Spi-ral-path high-sensitivity silicon photonic wiremolecular sensor with temperature-independent response. Opt. Lett. **33**(6), 596–598 (2008)

30. S. Kim, D. Baek, J.-Y. Kim, S.-J. Choi, M.-L. Seol, Y.-K. Choi, A transistor-based biosensor for the extraction of physical properties from biomolecules. Appl. Phys. Lett. **101**(7), 073703-1–073703-4 (2012)

31. H. Lou, L. Zhang, Y. Zhu, X. Lin, S. Yang, J. He, M. Chan, A junctionless nanowire transistor with a dual-material gate. IEEE Trans. Electron. Devices **59**(7), 1829–1836 (2012)

32. P. Razavi, A. A. Orouji, Dual material gate oxide stack symmetric double gate MOSFET: improving short channel efects of nanoscale double gate MOSFET. In: Electronics Conference, 2008. BEC 2008. 11th International Biennial Baltic, IEEE, pp. 83–86 (2008)

33. P. Kasturi, M. Saxena, M. Gupta, R.S. Gupta, Dual material double-layer gate stack SON MOSFET: a novel architecture for enhanced analog performance-part I: impact of gate metal workfunction engineering. IEEE Trans. Electron. Devices **55**(1), 372–381 (2008). https://doi.org/10.1109/TED.2007.910564

34. W. Long, H. Ou, J. Kuo, K.K. Chin, Dual-material gate (dmg) ield efect transistor. IEEE Trans. Electron. Devices **46**(5), 865– 870 (1999)

35. R. K. Baruah, R. P. Paily, A dual-material gate junctionless transistor with high- k spacer for enhanced analog performance. IEEE Trans. Electron. Devices **61**(1), 123–128 (2014)

36. A. Chakraborty, A. Sarkar, Analytical modeling and sensitivity analysis of dielectric-modulated junction-less gate stack surrounding gate MOSFET (JLGS-SRG) for application as biosensor. J. Comput. Electron. **16**, 556–567 (2017)